Advanced Turbulence and Combustion Modeling for the Study of a Swirl-Assisted Natural Gas Spark-Ignition Heavy-Duty Engine

Corresponding author: M. Riccardi[1,2], PhD Candidate (marco. riccardi@unina.it)
V.De Bellis[2], Associate Professor (vincenzo.debellis@unina.it),
L. Sforza[3], Researcher (lorenzo.sforza@polimi.it),
C. Beatrice[1], Researcher (c.beatrice@stems.cnr.it),
F. Bozza[2], Full Professor (fabio.bozza@unina.it),
M. Mirzaeian[4], Performance Simulation team leader
(mohsen.mirzaeian@cnhind.com),

1. CNR – STEMS, Via G. Marconi, 4, 80125 Naples, Italy
2. University of Naples "Federico II", Naples, Italy, +39-0817683264-3274
3. Polytechnic of Milano, via Lambruschini 4a, 20156 Milan, Italy
4. FPT Industrial S.p.A., Via Puglia 15, 10156 Turin, Italy

Declaration of interests

Credit Author Statement

Marco Riccardi: Conceptualization, Methodology, Software, Writing - Original Draft, Visualization. **Vincenzo De Bellis:** Conceptualization, Methodology, Software, Writing – Original Draft, Visualization, Supervision. **Carlo Beatrice:** Conceptualization, Methodology, Review & Editing. **Fabio Bozza:** Conceptualization, Methodology, Review & Editing. **Lorenzo Sforza:** Methodology, Writing. **Mohsen Mirzaeien:** Methodology, Resources.

Article Highlights

- Phenomelogical turbulence and combustion 0D/1D models for heavy-duty engines
- Turbulence model for large bore swirl-assisted engine
- Fractal combustion applied on a Natural Gas fuelled heavy-duty engine
- Experimental and numerical excellent comparison for different load and speed levels

Abstract

Increasing demands on higher performance and lower fuel consumption and emissions have led the path for internal combustion engine development; this race is nowadays directly related to CO2 emissions reduction. To drive engine development and reduce the time-to-market, the employment of numerical analysis is mandatory. This requires a continuous improvement of the simulation models toward real predictive analyses able to reduce the experimental R&D efforts.

In this framework, 1D numerical codes are fundamental tools for system design, energy management optimization, and calibration. The present work is focused on the improvement of the phenomenological turbulence model, originally conceived to describe turbulence evolution in tumble-promoting engines.

The turbulence model is developed with reference to a SI heavy-duty CNG engine derived from a diesel engine. In this architecture, due to the flat cylinder head, turbulence is also generated by swirl and squish flow motions, in addition to tumble motion. The presented turbulence model is validated against 3D CFD results, demonstrating to properly predict turbulence and swirl/tumble evolution under two different operating conditions, without the need for any case-dependent tuning.

The developed turbulence model is coupled to a phenomenological combustion model based on the fractal geometry theory applied to the flame front surface, where the turbulence is assumed to support flame propagation through an enhancement of the flame front area with respect to the laminar counterpart. The combustion model is validated against an extensive experimental dataset, composed of 25 operating points at different engine rotational speeds and loads. The numerical/experimental comparisons of global performance parameters are satisfactory, leading to maximum errors around $\pm 2\%$ for the BSFC, ± 2 deg for the main combustion events, and ± 1 bar for the in-cylinder peak pressure. Burn rate profiles are very well captured by the combustion model at changing operating conditions, not requiring any case-dependent tuning. The presented results demonstrate that the turbulence/combustion models could constitute a reliable virtual test facility, contributing to supporting and driving experimental activities.

1. Introduction

Since the 1950s, the economic growth generated by industrial development has derived an unprecedented and accelerating human-induced global change with a significant impact on air pollution and consequent health risks [1]

The increasing demand for low-emission and high efficiency of Internal Combustion Engines (ICE), together with the need of reducing time to market, has led to the development of more and more advanced design tools.

Greenhouse gases like carbon dioxide (CO_2) emitted due to road transport account for almost 26% of total CO_2 emissions from European Union in 2020 [2]. Other emissions are also known to be harmful to human health. For example, soot emitted from Diesel engines, which was previously classified as probably carcinogenic to humans in 1988, was, in 2012, reclassified as carcinogenic to humans (group 1) by an agency under the World Health Organization [3].

The solution to these ambitious challenges requires a series of harmonized actions, such as a growing share of renewable sources, the reduction of carbon fuel use, improvements in energy conversion efficiency, and structural changes in the economy, all driven and supported by the introduction of stringent legislation.

Regarding Heavy-Duty (HD) commercial vehicles the Compressed and Liquefied Natural Gas (CNG and LNG), nowadays, and the bio-methane (bio-NG) and Power-To-Gas methane (PTG) in the future, represent high potential co-solutions to match the mid-term and long-term neutral climate targets [4, 5, 6].

In this situation, it is essential to maintain affordable engine development costs. Companies, as well as researchers, utilize powerful software tools in conjunction with experimental investigations for this reason. From this perspective, it is essential to have mathematical models that can describe the various engine phenomenologies.

Before the actual prototyping of ICEs, a variety of computer simulation tools are available to estimate their performance with varying degrees of precision. Depending on the desired level of detail, these simulation tools may be based on three-dimensional (3D), one-dimensional (1D), or zero-dimensional (0D) models.

The purpose of this study is to contribute to the class of turbulence phenomenological models by describing the evolution of turbulence within the cylinder of an ICE. Following the validation of the turbulence model against the results of 3D-CFD simulations, the turbulence model is coupled with a predictive combustion model.

Turbulence is one of the most important aspects in Spark Ignition (SI) engines as it can significantly affect burn rates, heat transfer rates, and combustion stability, and thus performance.

Turbulence originates from a large-scale motion that occurs during the induction process, which mainly consists of tumble motion in modern SI engines with a pentroof cylinder head. Despite its significance, most of the 0D turbulence models rely on calibration factors when calculating the evolution of tumble motion and its conversion into turbulence.

It is commonly understood that tumble motion contributes to the improvement of flame front velocity in SI engines. When the piston is near TDC, the tumble motion diminishes, resulting in an increase in the Turbulent Kinetic Energy (TKE).

Most of CNG SI Heavy-Duty engines are derived from diesel engines, and properly converted to operate under SI mode. The combustion chamber is commonly located in the piston crown and a flat cylinder head is used [7]. In the case of a flat cylinder head with a bowl piston, tumble and swirl are both fundamental to the development of the turbulent motion field and the squish plays an important role, especially near the TDC. By fragmenting these flows into small-scale turbulent eddies, swirl, tumble, and squish flows increase the intensity of turbulence during late compression. This accelerates the rate of combustion and enhances the speed of turbulent flames [8].

The current literature presents various 0D phenomenological approaches to face the prediction of turbulence, most of them classified as k-ε and K-k models, where K and k are the mean and turbulent kinetic energy and ε is the turbulent dissipation rate. The

original proposals of k-ε models are reported in [9, 10], in which 0D equations of TKE, k, and dissipation rate, ε, are derived from 3D models. A preliminary attempt to consider the effect of ordered flow structures on turbulence is proposed in [11] in which source terms, related to the swirl and squish motions, are introduced. K-k models are a different method for analyzing the energy cascade mechanism that occurs between the mean and turbulent flow fields. In [12] a K-k model is developed, computing both tumble and swirl motions and their dissipation in turbulence, where the critical issue is the description of the flow structure decay during the compression stroke, due to the shear stresses. A more comprehensive approach is proposed in [13], which synthesizes the K-k and k-ε models, resulting in the so-called K-k-ε model, and describes directly the turbulence dissipation.

Authors have made significant improvements to the family of K-k models [14, 15, 16], which demonstrated to properly sensing both the engine operating parameters, including the intake valve strategy and the engine geometrical features. In [18] the authors have extended the study, including the formulation of tumble and dissipation rate, resulting in the so-called K-k-T model, in which T is the tumble-associated specific angular momentum.

The tumble motion directly affects the TKE in SI engines and the focus was primarily on developing flow models that consider tumble as the main promoter for turbulence generation and combustion enhancement [17]. Heavy-Duty SI engines fueled with CNG are mostly Diesel-derived, so the inlet flow motion is more similar to a Compression Ignition (CI) engine. For this reason, in the authors' perspective, the development of a 0D model that accounts for all the sources of turbulence generation, that are tumble, swirl, and squish motion, appears attractive.

The turbulence model is used as a user sub-pattern in the fractal predictive combustion model [19]. This predictive combustion model was largely used in 0D/1D engine simulations, demonstrating its good predictive capabilities, after a proper calibration [19, 20]. Predictive models self-adjust for transient conditions and also the spatial resolution could give more detailed output (i.e. NOx, knock, heat transfer).

Various combustion models for Spark-Ignition (SI) have been proposed for many years [21,22], trying to physically describe the main in-cylinder phenomena. Some of them are employed in proprietary or commercial 1D codes. Basic differences between them consist in the way the laminar-turbulent flame transition occurs and in the mechanism inducing the turbulence-related burn-rate enhancement [23,24]. Other approaches are also used, such as the one introduced in [25], where the combustion chamber is described as a stochastic reactor and the combustion is modeled by probability density functions.

One of the most successful combustion models is the eddy burn-up model. It describes the flame entrainment and subsequent combustion of the unburned mixture and proved to agree with the experimental burned mass fraction trends [26,27]. In this article, the fractal combustion model approach is used. The fractal model tries to directly estimate the flame front wrinkling and related effects on the burning rate, as reported in several publications [28, 29, 30].

The novelty of this work consists of the characterization of a 0D turbulence model adapted to an engine in which the swirl motion component is predominant. The

turbulence model has been developed with particular attention to the real flow evolution inside the cylinder during all the engine phases. In the literature, there is no turbulence model of this type, adapted for spark ignition large bore engines and fuelled with CNG.

The article is organized as follows. The next section presents the governing equations of the turbulence/flow model. This is followed by the description of the engine geometry and the setup of 3D-CFD runs that were used to calibrate and validate the proposed model. Subsequently, the fractal predictive combustion model is presented, explicating the link with the turbulence model. The combustion model is then validated against an extensive experimental dataset, in terms of global performance parameters and pressure cycle/burn rate profiles. The final section presents some conclusions of the current study and directions for future investigations.

2. Engine Description and Experimental test

The main features of the engine under study (Figure 1) are reported in Table 1. This engine is designed to guarantee long-distance when installed on heavy-duty trucks (over 16 tons of gross vehicle weight). It is a heavy-duty, turbocharged SI engine with a compression ratio of 12:1. The considered engine is retrofitted from a Compression Ignition (CI) application, through the installation of ported CNG injectors and spark-plugs. The CNG is injected through a Multi Point Injection (MPI) system, and it is metered to ensure a close-to-stochiometric air/fuel mixture in the combustion chamber. The load control is realized by the waste-gated turbocharger at mid/high load, and by the throttle valve at low load. An intercooler is located after the compressor to limit the inlet temperature of the air. Each cylinder is equipped with a centred spark-plug, and two intake and exhaust valves, both with fixed timing (Figure 2).
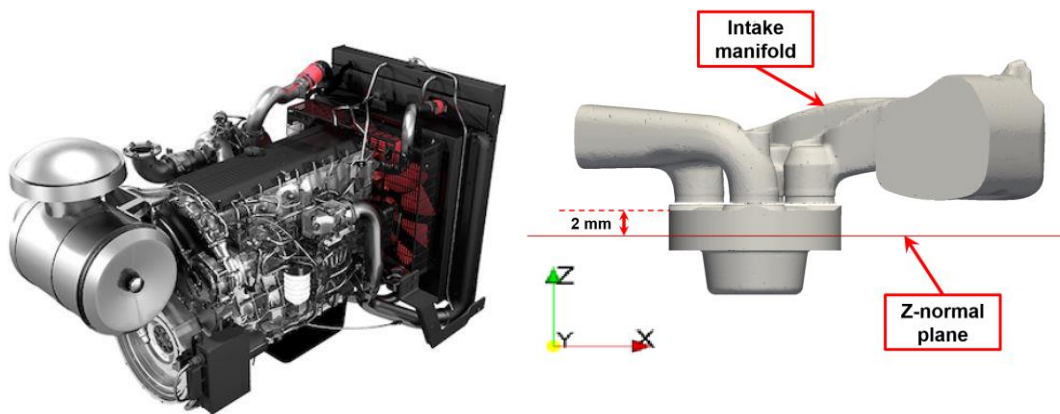

Figure 1 – Overview of the 6-cylinder engine under exam.

Figure 2 - Layout of the intake and exhaust systems, with the piston at the TDC position (numerical domain for the 3D-CFD simulations).

The experimental campaign is carried out at Istituto Motori (CNR), analyzing the engine at full- and part-load conditions. The engine is tested at five different speeds from 1100 up to 1900, for 5 different load levels. In total, 25 operating points, listed in Table 2, are investigated, identified by the couple engine speed and load (rpm@BMEP). For each condition, overall performance data, such as Brake Specific Fuel Consumption (BSFC), fuel rate, and emissions are collected. Additionally, the instantaneous pressure cycle is recorded through a pressure transducer, and post-

processed to derive the angular positions of representative combustion stages (spark event and 10%, 50% as well as 75% of Mass Fraction Burned).

Table 1. Main features of the selected CNG SI Heavy-Duty engine.

Turbocharged SI Engine	
Cylinder Arrangement	6l (in-line) vertical
Displacement, l	12.85
Compression Ratio	12:1
Stroke, mm	150 mm
Bore, mm	135 mm
Valves per cylinder	4
Bowl depth	~30 mm
Bowl radius	~37 mm
Average squish height	~2.5 mm @ TDC
Maximum brake power, kW	338 @ 1900 rpm
Maximum brake torque, Nm	2000 @ 1100 / 1620 rpm
Injection System	MPI
Valve number	4
IVO – IVC at 2 mm lift, CAD AFTDC	383-515
EVO – EVC at 2 mm lift, CAD AFTDC	146-333
External EGR	NO

Looking at combustion phasing in Table 2, expressed by the Crank Angle Degree (CAD) at which 50% of the mixture is burned (MFB_{50}), it is evident that the engine works at knock-limited conditions for the higher loads. Whereas for BMEP levels below 13 bar, the typical optimal MFB_{50} around 8-10 CAD is detected, which leads to the maximum brake torque.

Table 2. List of operating points.

Case	Operating condition	SA	MFB_{50}

	rpm @ BMEP [bar]		CAD BFTDC	CAD AFTDC
1		16.6	13.8	17.5
2		13.3	16.6	14.1
3	1900	10.0	23.5	7.5
4		6.6	26.2	6.6
5		3.3	25.8	9.7
6		19.4	11.3	19.0
7		15.6	13.4	16.4
8	1620	11.7	19.1	10.4
9		7.8	24.3	7.0
10		3.9	23.8	10.0
11		19.4	10.7	19.2
12		15.6	13.0	16.1
13	1500	11.7	18.7	10.3
14		7.8	23.0	7.5
15		3.9	23.8	10.0
16		19.5	9.9	18.4
17		15.6	12.2	15.2
18	1300	11.7	17.9	10.3
19		7.8	20.8	8.9
20		3.9	22.4	10.1
21		19.5	9.0	17.7
22		15.6	11.1	15.0
23	1100	11.7	16.7	9.9
24		7.8	18.3	9.9
25		3.9	19.7	11.3

3. 0D In-Cylinder flow model

A 1D model of the engine under study is developed within a 0D/1D modeling environment, where the engine is schematized through a network of 1D pipes and 0D volumes. The turbocharger system is handled by a standard map-based approach, whereas the in-cylinder phenomena are described by refined, in-house developed, phenomenological sub-models for turbulence, combustion, and heat transfer.

The K-k-T turbulence model, previously presented by authors [31], considered not only an equation for the kinetic energy of the mean flow, K, and one of the turbulent flow, k, but also an equation for the specific angular momentum of the tumble motion, T. In tumble-assisted SI engines, this model is highly recommended, but in the engine under exam, where the combustion chamber is in the piston crown and the cylinder head has a flat geometry, the flow motion during the intake phase is mainly governed by the swirl motion rather than tumble one.

$$\frac{dmK}{dt} = (\dot{m}K)_{inc} - (\dot{m}K)_{out} + mK\frac{\dot{\rho}}{\rho} - P - P_T - P_S + \dot{K}_{inj} \tag{1}$$

$$\frac{dmk}{dt} = (\dot{m}k)_{inc} - (\dot{m}k)_{out} + \frac{2}{3}\frac{\dot{\rho}}{\rho}\left(-mv_t\frac{\dot{\rho}}{\rho} + mk\right) + P + P_T + P_S - m\varepsilon \tag{2}$$

$$\frac{dmT}{dt} = (\dot{m}T)_{inc} - (\dot{m}T)_{out} - f_{dT}\frac{mT}{t_T} \tag{3}$$

$$\frac{dmS}{dt} = (\dot{m}S)_{inc} - (\dot{m}S)_{out} - f_{dS}\frac{mS}{t_S} \tag{4}$$

The equations shown above govern the evolution of the following flow quantities:

1. Mean kinetic energy $K = (1/2)U^2$, where U is the mean velocity inside the cylinder.

2. Turbulent kinetic energy $k = (3/2)u'^2$, where u' is the intensity of the turbulent field inside the cylinder, assumed to be homogeneous and isotropic.

3. Specific angular momentum of the tumble motion $T = U_T r_T$, where U_T is the tumble vortex velocity and r_T is the tumble radius. The kinetic energy K_T related to tumble momentum is $U_T^2/2$. Tumble speed is commonly expressed in a non-dimensional form as tumble number $N_T = U_T/(\omega_{eng} r_T)$, where ω_{eng} is the engine angular speed.

4. Specific angular momentum of the swirl motion $S = U_S r_S$, where U_S is the swirl vortex velocity and r_S is the swirl radius. The kinetic energy K_S related to

swirl momentum is $U_S^2/2$. As well as tumble number, swirl number is defined as: $N_S = U_S/(\omega_{eng}r_S)$.

The term m is the in-cylinder mass, while $\dot{K}_{inj}$ is the kinetic energy associated with possible direct fuel injection.

3.1 Convective flows

The first and the second term in the above equations describe incoming and outcoming convective flows through the valves. The following equations are used:

$$(\dot{m}K)_{inc} = \frac{1}{2}\left[\dot{m}_{inf}\left(c_{Kin0}v_{Kinf}\right)^2 + \dot{m}_{exf}v_{Kexf}^2 + \dot{m}_{exb}v_{Kexb}^2\right] \tag{5}$$

$$(\dot{m}K)_{out} = K(\dot{m}_{inb} + \dot{m}_{exf}) \tag{6}$$

$$(\dot{m}k)_{inc} = 0 \tag{7}$$

$$(\dot{m}k)_{out} = k(\dot{m}_{inb} + \dot{m}_{exf}) \tag{8}$$

$$(\dot{m}T)_{inc} = r_T\left(\dot{m}_{inf}c_{Tin0}v_{Tinf} - \dot{m}_{exf}v_{Texf} - \dot{m}_{exb}v_{Texb}\right) \tag{9}$$

$$(\dot{m}T)_{out} = T(\dot{m}_{inb} + \dot{m}_{exf}) \tag{10}$$

$$(\dot{m}S)_{inc} = r_S(\dot{m}_{inf}c_{Sin}v_{Sinf} - \dot{m}_{exf}c_{Sex}v_{Sexf} - \dot{m}_{exb}v_{Sexb}) \tag{11}$$

$$(\dot{m}S)_{out} = S(\dot{m}_{inb} + \dot{m}_{exf}) \tag{12}$$
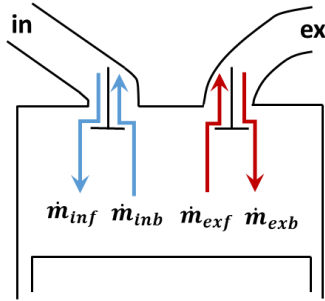

Figure 3 – Schematic of valve flows.

In the Equations above $\dot{m}_{in}$ and $\dot{m}_{ex}$ indicate the mass flow passing through the intake and exhaust valves, respectively. The subscripts f and b indicate the directions of the flow through the valves, that can be forward or backward (Figure 3). Instantaneous mass flows are calculated through a simple nozzle-like model, accounting for the pressure difference across the valve and the effective flow area, related to the instantaneous flow coefficient and valve lift.

In Equations 5, 9, and 11, the velocities v_K, v_T and v_S include the flow losses through the valves. More precisely, they comprise the discharge, the tumble, and the swirl coefficients, respectively. These coefficients are automatically specified as a function of the valve lift. Even if the model does not explicitly describe the actual shape of

intake runners, the influence of intake port design on ordered and unordered motions is considered in the above coefficients. The possibility to tune the discharge, tumble, and swirl momentum is offered by the global multipliers c_{Kin0}, c_{Tin0}, $c_{Sin,}$ and c_{Sex}. The last two terms of Equations 9 and 11 give a subtractive contribution to the tumble and swirl intensities, assuming that the exhaust flow, both in forward and backward direction, produces a reverse tumble and swirl, opposite to the ones produced by intake flows.

3.2 Decay functions

In the Equations 3 and 4, the terms $f_{dT}\frac{mT}{t_T}$ and $f_{dS}\frac{mS}{t_S}$ express the decay of the two main ordered motions due to the shear stresses with the combustion chamber walls. A decay function f_d is used for the tumble and another one for the swirl, considering a characteristic time scale t_T for the tumble and t_S for the swirl.

$$f_{dT} = c_{fd0,T} + c_{fdm,T}\left[\max\left(\frac{B}{H},1\right)-1\right] \tag{13}$$

$$t_T = \frac{r_T}{u'} \tag{14}$$

$$f_{dS} = c_{fd0,S} + c_{fdm,S}\left|\frac{U_{sq}}{U_S}\right| \tag{15}$$

$$t_S = \frac{r_S}{u'} \tag{16}$$

Both decay functions for tumble and swirl are dependent on a fixed term and a time-varying term. The former is active during the whole engine cycle and expresses the dissipation of ordered flow structures caused by internal viscous forces, while the latter takes into account the dissipation effects caused by the piston rising (Figure 4 andFigure 5). Specifically, the second term of tumble decay indicates its collapse caused by the piston rising, and it is inversely proportional to the piston position, H, normalized by the cylinder bore, B (Figure 4). This component is supposed to be proportional to the ratio of the squish velocity, U_{sq}, to the swirl velocity, U_S. To adjust the two contributions to tumble and swirl decays, Equations 13 and 15 present two parameters, $c_{fd0,x}$ and $c_{fdm,x}$. Equations 14 and 16 show that the characteristic time scales, t_T, and t_S, of tumble and swirl are assumed to inversely depend on the turbulence intensity and directly on the related radii. The radii of tumble and swirl are calculated based on geometrical data of the cylinder and piston according to Equations 17 and 18.
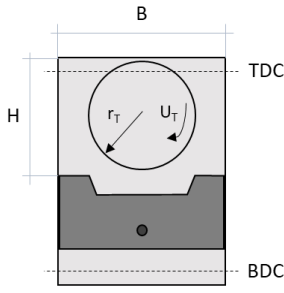
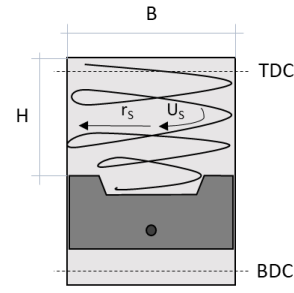**Figure 4** - Qualitative sketch of the tumble vortex.

Figure 5 - Qualitative sketch of the swirl vortex.

$$r_{T,S} = c_{r0T,S} + c_{rmT,S} \frac{1}{4} \sqrt{B_\vartheta^2 + (H + s_{bowl})^2} \tag{17}$$

$$B_\vartheta = \frac{(V_{cyl} - V_{bowl}) \cdot B + V_{bowl} \cdot d_{bowl}}{V_{cyl}} \tag{18}$$

In Equation 17, B_θ and ($H+s_{bowl}$) are instantaneous representative dimensions along radial and axial directions around which ordered motions arise, whereas c_{r0T} and c_{rmT} (or c_{r0S} and c_{rmS}) are two parameters that allow the tumble (or swirl) radius to be adjusted. d_{bowl} and s_{bowl} are the diameter and the height of the piston bowl, respectively (Figure 6). B_θ is a time-variant parameter (Equation 18), it is equal to the bore B if the piston is at BDC, while it is equal to the bowl diameter if, ideally, there is no space between the top of the piston and the cylinder head. In the Equation 18, V_{cyl} is the instantaneous cylinder volume, and V_{bowl} is the piston bowl volume.

The mean velocity of the squish motion inside the cylinder, U_{sq}, is quantified by Equation 19 [33]. This velocity depends in turn on its axial, U_a, and radial, U_r, components that are related to main geometric characteristics of the cylinder and piston bowl and on the cylinder volume variation rate.

$$U_{sq} = \frac{1}{3}\left(U_r \left(1 + \frac{d_{bowl}}{B}\right) + U_a \left(\frac{d_{bowl}}{B}\right)^2 \right) \tag{19}$$

$$U_r = \frac{dV_{cyl}}{dt} \cdot \frac{V_{bowl}}{V \cdot (V_{cyl} - V_{bowl})} \cdot \frac{B^2 - d_{bowl}^2}{4d_{bowl}} \tag{20}$$

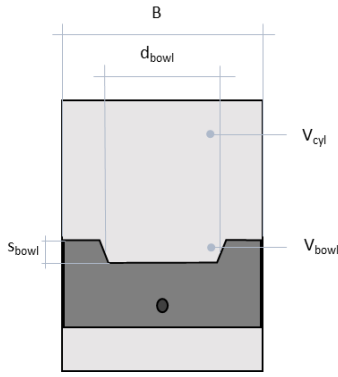$$U_a = \frac{dV_{cyl}}{dt} \cdot \frac{s_{bowl}}{V} \tag{21}$$

Figure 6 - Qualitative sketch of the main geometrical data of cylinder and piston.

3.3 Production term

The energy cascade mechanism is modelled by the terms P, P_S and P_T in Equations 1-2. Those terms are subtractive for the kinetic energy K associated to the mean flow, while they are additional terms for the turbulent kinetic energy k.
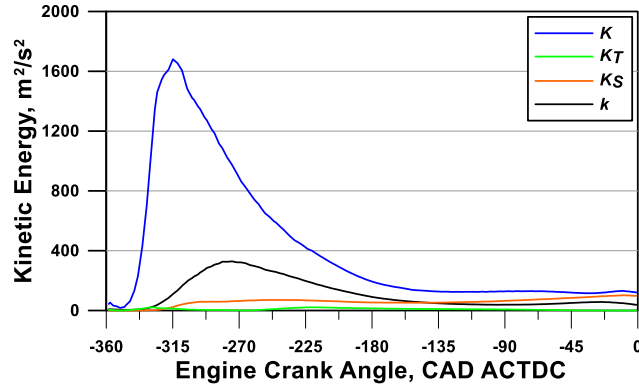

Figure 7 - Kinetic energies associated to mean, tumble, swirl and turbulent flows.

Since most of the flow structures generated during the intake phase are unordered, the mean flow kinetic energy is significantly greater than the tumble and swirl-associated kinetic energies. In the engine design under study, the tumble motion is weak while the swirl motion is prominent. Due to the conservation of angular momentum, the swirl vortex velocity increases as the piston rises, and the swirl radius decreases as a result of the flow motion entering the piston bowl. Due to the high swirl vortex velocity, shear stresses and internal viscous forces increase the turbulence kinetic energy close to the TDC (Figure 7).

The turbulent production due to unordered flows is computed by the difference between the overall mean flow kinetic energy K and the ones associated to the two ordered flow motions, K_T and K_S.

$$P = c_{PKk} m \frac{K - K_T - K_S}{t_{TS}} \tag{22}$$

In the Equation above c_{PKk} is a tuning constant to modulate the energy transfer from the mean flow to the turbulent one, t_{TS} is a characteristic time scale determined by a

weighted average, Equation 23, depending on tumble and swirl intensities, Equation 24.

$$t_{TS} = wt_T + (1 - w)t_S \qquad (23)$$

$$w = \frac{|U_T|}{\sqrt{U_T^2 + U_S^2}} \qquad (24)$$

Ordered motions also contribute to turbulence production depending on their dissipation rates, modelled by the last terms in Equations 3 and 4. The productions of turbulent kinetic energy related to tumble and swirl decays are evaluated by differentiating tumble- and swirl-related kinetic energy definitions, as reported below:

$$P_X = \frac{U_X}{r_X}\left(f_{dX}\frac{mX}{t_X}\right) \qquad (25)$$

where X indicates either swirl or tumble.

3.4 Dissipation term

In the Equation 2, the dissipation rate ε is determined through the Equation 26.

$$L_i = c_\mu^{3/4}\frac{k^{3/2}}{\varepsilon} \qquad (26)$$

where c_μ is a constant and L_i is the turbulence integral length scale. As demonstrated in prior research [16], this value varies marginally depending on the engine operations (speed, load, valve strategy, etc.), but largely depends on the engine type and combustion chamber shape. For this reason, the authors have opted to impose a sequence of S-shaped functions to describe the evolution of L_i during the engine cycle. The parameters of these functions are chosen to accommodate the *Li* trend accord to results of 3D simulations.

4. Results and discussion on turbulence model

This section presents the predictions of the proposed 0D flow/turbulence model at 2 operating conditions and compares them to the results obtained via 3D-CFD simulations, widely detailed in [34]. The operating conditions considered are at 1200 rpm and 1900 rpm, whose main engine settings are listed in Table 3.

The 3D-CFD simulations of the gas exchange process were performed with Lib-ICE software, which is a code based on the OpenFOAM technology and extensively used for simulating IC engines for both academical and industrial tasks [35, 36, 37]. The tumble and swirl radii, r_T and r_S, derived from 3D analyses are here defined as:

$$r_T = \frac{\sum_{cyl} m_i[(x_i - x_G)^2 + (z_i - z_G)^2]}{\sum_{cyl} m_i \sqrt{(x_i - x_G)^2 + (z_i - z_G)^2}} \qquad (27)$$

$$r_S = \frac{\sum_{cyl} m_i [(x_i - x_G)^2 + (y_i - y_G)^2]}{\sum_{cyl} m_i \sqrt{(x_i - x_G)^2 + (y_i - y_G)^2}} \qquad (28)$$

where m_i is the mass in the ith cell; x_i, y_i, z_i are the Cartesian coordinates of the ith cell center; and x_G, y_G, z_G are the Cartesian coordinates of the in-cylinder mass center. The tumble and the swirl radii are here defined around the y-axis and z-axis, respectively (see Figure 2).

A mono-cylindrical 1D model of the engine under study is developed within a commercial software (GT-Power) based on a 0D/1D modeling environment, where the engine is schematized through a network of 1D pipes and 0D volumes. The 0D flow/turbulence pattern is implemented as user sub-model using GT-Power tools and it ran in motored conditions just to evaluate the cold flow impact on turbulence generation, with no combustion influence.

Table 3 - The investigated operating conditions.

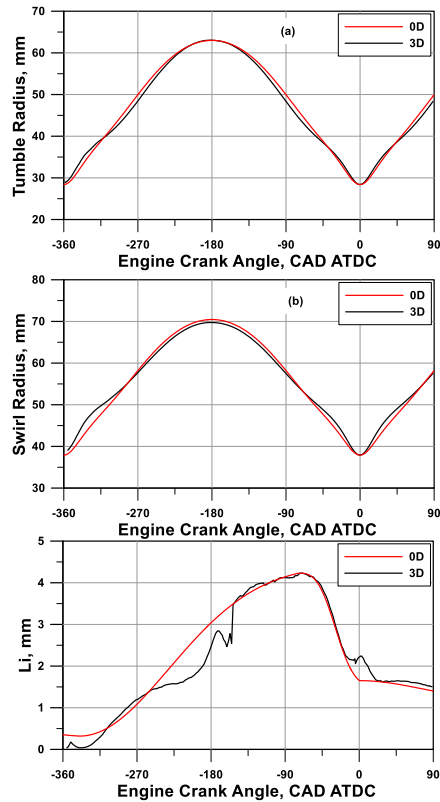| Operating condition	*Cruise*	*Max power*
Engine speed [rpm]	1200	1900
Brake torque [Nm]	850	1700
Brake power [kW]	100	338
Air-fuel ratio λ	1	1
EGR [%]	14.5	11.2

Figure 8 - Comparison between 3D-CFD and 0D results of tumble (a) and swirl (b) radii and normalized integral length scale (c).

The flow/turbulence model is tuned manually through a simple trial and error procedure to obtain a good match of all quantities of interest with 3D results. These last are synthesized in scalar quantities through mass-averaging process within the cylinder. Since 3D simulations started at the beginning of the exhaust phase, with null initial swirl, and covered a single engine cycle, a full cycle-by-cycle convergence is not reached. All the 0D/3D comparisons presented below cover intake, compression and a portion of expansion stroke, when cyclic convergence can be assumed adequate. The values of the flow/turbulence model constants after the tuning are listed in the Table 4. They are kept fixed for the tested operating conditions, with no case-dependent specific tuning.

As stated previously, in this K-k-T-S model, some variables, particularly those pertaining to the geometrical properties of the engine and combustion chamber, are not estimated but rather imposed based on established patterns. Using Equation 17, the radii of tumble and swirl are determined by modifying the c_{r0X} and c_{rmX} parameters to match the 3D levels at BDC and TDC, respectively. Similarly, the integral length scale is computed by assigning levels at certain angular points (firing TDC, minimum and maximum levels during intake and compression strokes). Figure 8 demonstrates that the 0D patterns properly match the 3D counterparts, particularly during the intake and compression strokes, which are the most significant phases for a good forecast of combustion. 3D-CFD simulations revealed no notable variations in the outcomes of tumble/swirl radius and integral length scale for the two analyzed engine rotational speeds. Thus, 0D/3D assessment is only presented for the speed of 1900 rpm.

Table 4 - Values of flow model tuning constants.

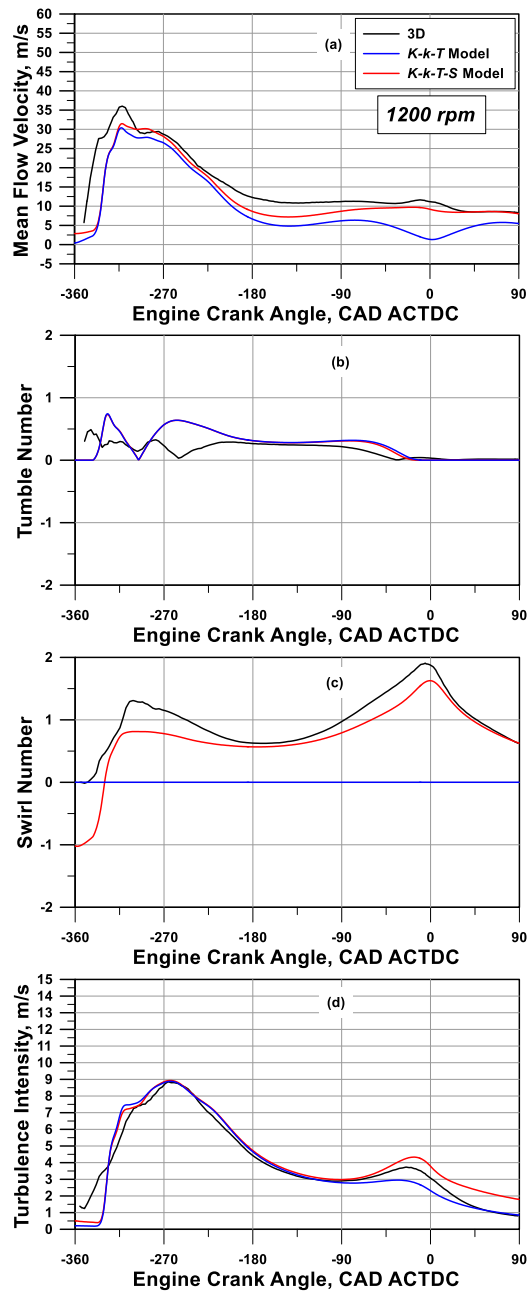| Tuning constant	Value	Tuning constant	Value
c_{Kin0}	0.60	c_{Sin}	0.08
c_{Tin0}	0.45	c_{Sex}	0.02
$c_{fd0,T}$	0.55	$c_{fd0,S}$	0.05
$c_{fdm,T}$	1.0	$c_{fdm,S}$	1.0
c_{PKk}	3.5		

Figure 9 - Comparison between 3D-CFD and 0D results at 1200 rpm of mean flow velocity (a), tumble number (b), swirl number (c) and turbulence intensity (d).

Figure 9 andFigure **10** shows that the overall behavior of the model is quite satisfactory in the comparison with 3D outcomes, for both the analyzed operating conditions. The mean flow velocity, the tumble number, the swirl number, and the turbulence intensity denote a very good agreement with the related 3D profiles, during most of the engine cycle. The mean flow velocity, tumble and swirl, increases during the intake phase due to incoming flow through the intake valve. According to expectations, those velocities appropriately scale with engine rotational speed, passing from 1200 rpm to 1900 rpm. After a partial decay during the ending part of the intake phase, mean flow velocity persists and even accelerates near TDC because of the swirl motion speeding up. The swirl radius reduces, approaching the TDC, due to the smaller volume available in the combustion chamber, so for the angular momentum conservation, the swirl velocity

enhances. The squish is not directly described by a dedicated equation, but its effects are indirectly taken into account as energy lost in the decay of the swirl.
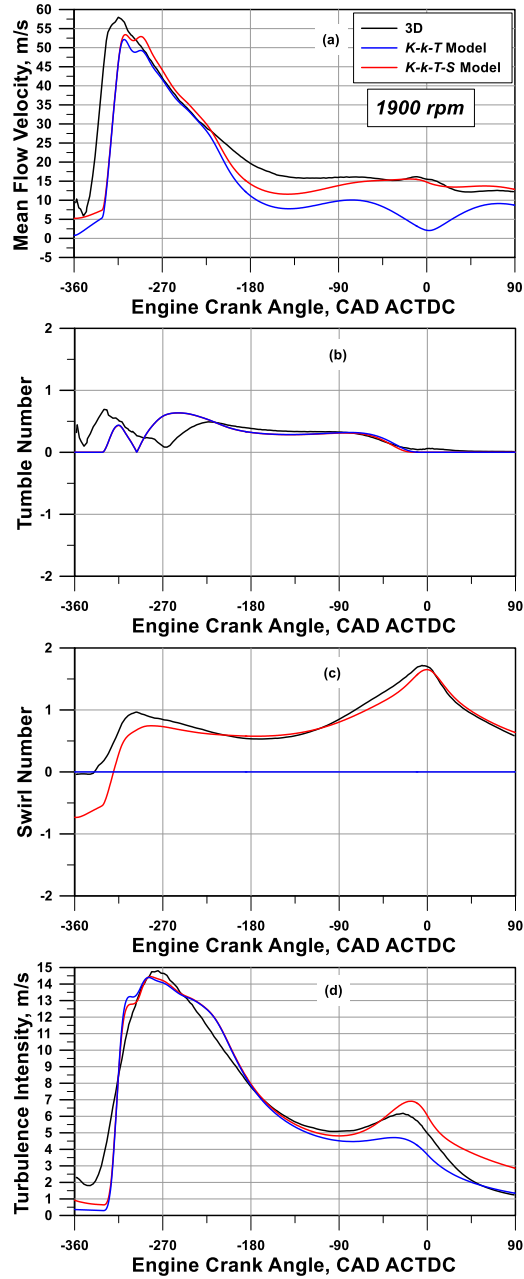

Figure 10 - Comparison between 3D-CFD and 0D results at 1900 rpm of mean flow velocity (a), tumble number (b), swirl number (c), and turbulence intensity (d).

As emerged from 3D analyses, tumble momentum presents comparable components around two principal axes (x-axis and y-axis) perpendicular to the cylinder symmetry axis (z-axis). For this reason, those momentum components are combined according to:

$$T_{XY} = \sqrt{T_X^2 + T_Y^2} \qquad (29)$$

For sake of consistency, the absolute values of 0D-computed tumble number are compared to 3D results in Figure 9b and Figure 10b. The 0D prediction appears quite poor during the intake phase, and this is due to its incapability to reproduce multiple and unstructured tumble eddies generated during this phase in the engine under study [34]. The model accuracy drastically improves during the compression stroke, where tumble collapse towards TDC is quite well captured.

Figure 9 andFigure **10** also depict the comparisons between the results of the presented *K-k-T-S* model and the ones of the *K-k-T* variant. The figures show that the novel model allows obtaining a better prediction of mean flow kinetic energy around the FTDC. On the opposite, the *K-k-T* model does not perceive the effect of swirl motion in sustaining the mean flow velocity when the piston moves around the FTDC. This reflects in an improved turbulence estimation by the *K-k-T-S* model, especially for the higher rotational speed.

Looking at Figure 9b-c and Figure 10b-c, the tumble and swirl number profiles are overall satisfactorily reproduced during most of the engine cycle, with a higher accuracy towards the ending portion of the compression stroke, when the contribution of those motions to turbulence generation become more relevant. The turbulent intensity is satisfactorily predicted in the 0D pattern over the considered portion of the engine cycle. During the intake phase and the early stage of the compression stroke, 0D turbulence prediction mainly relies on accuracy in the simulation of mean flow velocity. Near to the TDC, the characteristic speed-up of turbulence intensity is captured by the model through the cascade mechanisms of kinetic energy from unordered and ordered flows to smaller scales.

5. Fractal Combustion model

The turbulence model above presented is combined with a predictive combustion model, developed at the University of Naples in the last years [19]. This model assumes that the aerodynamic turbulence enhances the burn rate with respect to the one occurring under a laminar propagation, through an increased surface of the flame front. In particular, the fractal model directly describes the enhancement of this increased flame front surface, resorting to the concepts of fractal geometry. Experimental observations proved, indeed, that a wrinkled flame front presents a fractal behaviour, resulting in the auto-similarity of its basic structure [38, 39]. This gives the possibility to relate the turbulent flame front extent to the laminar one according to turbulence characteristic speed, time, and length scales. Under this assumption, the burning rate is expressed as:

$$\left(\frac{dm_b}{dt}\right)_{fractal} = \rho_u A_T S_L = \rho_u A_L S_L \left(\frac{A_T}{A_L}\right) = \rho_u A_L S_L \left(\frac{L_{max}}{L_{min}}\right)^{D_3-2} \tag{30}$$

ρ_u is the unburned gas density, A_L and A_T are the area of the laminar and turbulent flame front areas, and S_L is the laminar flame speed. For the A_L estimation, a tabulated approach is followed. To this aim, in a preliminary stage, an off-line procedure calculates the intersections between a smooth spherically shaped flame front centred at the spark plug, and a simplified geometry of the combustion chamber. A look-up table is created, which collects, at each piston position and flame radius, the burned gas volume and the flame front surface area. The above table is loaded and interpolated at run-time, based on the current piston position and burned gas volume. The flame

speed, S_L, is evaluated by an empirical correlation as a function of the thermodynamic state, equivalence ratio, and charge dilution, detailed in the next section. L_{max} and L_{min} are the length scales of the maximum and minimum flame wrinkling. The former, (L_{max}) is related to a macroscopic characteristic dimension of the flame front, function of the flame radius, the latter (L_{min}) is taken equal to the size of the smallest turbulent eddy, namely the Kolmogorov length scale. This last, as well known, depends on the turbulence intensity and the integral length scale. Whereas, D_3, defined as the flame front fractal dimension, is assumed to depend on turbulence intensity, u', and laminar flame speed, S_L, by an empirical correlation, reported in [40].

The estimation of L_{max}, L_{min} and D_3 is based on the dedicated turbulence sub-model above presented. Eq. (30) applies to fully developed and freely propagating turbulent flame. Concerning the early flame development, a transition from laminar to turbulent combustion is introduced, as a function of a characteristic time scale of the turbulent flow field [41]. Whereas, for the combustion tail, a flame-wall interaction is taken into account ~~according to [41]~~, assuming a weighted average between a purely fractal burning rate and a laminar wall combustion. The laminar flame speed, S_L, is here estimated by the correlation presented in [42, 43, 44]. This is computed by the 1D simulations of planar flames burning pure methane in the air under wide ranges of pressure, temperature, and equivalence ratios. Those levels are in line with the ones occurring in the engine under study.

The summarized fractal combustion model has been successfully applied to light-duty and high-performance gasoline engines in the past [45, 46, 47]. In addition, in [41] it has been compared, in terms of tuning efforts and predictive accuracy, to well-known approaches, such as the eddy burn-up model [48, 49]. The authors in [41] found that the fractal model is characterized by a reduced constant-to-constant cross-dependency, producing lower tuning efforts with respect to the eddy burn-up model. Each tuning parameter in the fractal model is designed to exert a local effect during a single phase of the combustion process (laminar-turbulent transition, fully turbulent flame propagation, and wall/flame interaction). Additionally, during the present activity, some preliminary calculations showed that the fractal model, at partial load, exhibited higher reliability in predicting the experimental data, in terms of both engine performance and burn rate shape, without the need to adjust any tuning parameter.

These advantages are justified by the theoretical background of the fractal approach, since it is more directly founded on the combustion regime occurring in a SI engine, falling in the wrinkled-corrugated flamelets zone [50]. Indeed, the fractal model directly describes the enhancement of the flame front surface due to its interaction with the turbulence, reproducing the observations reported in several experimental activities [40-51]. As a final remark, it is worthwhile mentioning that the fractal combustion model is implemented, as well as the presented turbulence model, in the GT-Power environment under the form of user coding.

Concerning other modelling features, the Woschni correlation is adopted for the wall heat transfer modelling, as reported in [8]. Although knock phenomena occur for the considered CNG SI engine at the higher loads, at this stage of the research, this process is not simulated, focusing the study mainly on the validation of the combustion model.

6. Engine model set-up, tuning, and validation

6.1 Model set-up

A 1D model of the engine under study is developed within a 0D/1D modelling environment, where the engine is schematized through a network of 1D pipes and 0D volumes. The turbocharger system is handled by a standard map-based approach, whereas the in-cylinder phenomena are described by refined, in-house developed, phenomenological sub-models for turbulence, combustion, and heat transfer.

To reproduce in the 1D model the same operating conditions experienced in the experimental campaign, some control parameters are imposed as a simulation input. More specifically, the fuel is automatically metered to match the measured air/fuel ratio, whereas two PIDs are introduced for load control. The former acts on the turbocharger wastegate opening, which targets the measured boost level. The latter modifies the throttle valve position, following the measured BMEP level. The experimentally-derived MFB_{50} is imposed in the simulations, iteratively adjusting the SA at run-time, until the prescribed MFB_{50} is matched.

Although different correlations/models for the estimation of the friction losses are available in the current literature, at this stage of the activity, the experimental FMEP data are imposed in the 1D simulation.

6.2 Model tuning

The combustion model is firstly tuned at full load, to minimize the overall speed-averaged error between the computed and experimental characteristics combustion angles. To this aim, 3 tuning constants have to be specified, each of them acting, as said, on a specific phase of the combustion process, namely the transition between an initially laminar to a fully-turbulent combustion, the fully-developed flame wrinkling, and the combustion tail. Using a trial-and-error procedure, a single set of tuning constants is identified, following the steps presented in [41].

In Figure 11, the results of the full-load tuning procedure are reported in terms of characteristic combustion events, namely SA, MFB_{10}, MFB_{50}, and MFB_{75}. Since the MFB_{50} is imposed in the calculations, the combustion model accuracy can be mainly appreciated in terms of experimental/numerical comparison on the SA.

A slow initial burning rate, expressed as [MFB_{10}-SA] duration, is evident in the results. Being the considered engine retrofitted from a CI application, a low turbulence level is established inside the combustion chamber, which lengthens the transition from an initially laminar to a fully-turbulent combustion. Since the phenomenon is directly considered in the model, a good match of both the SA and the MFB_{10} can be observed. The burning speed during the combustion core, expressed in terms of [MFB_{50}- MFB_{10}], is also very well reproduced. Since the MFB_{90} is always hard to measure experimentally due to the inaccuracy to catch the end of combustion, MFB_{75} is considered to adjust the speed of the combustion tail.
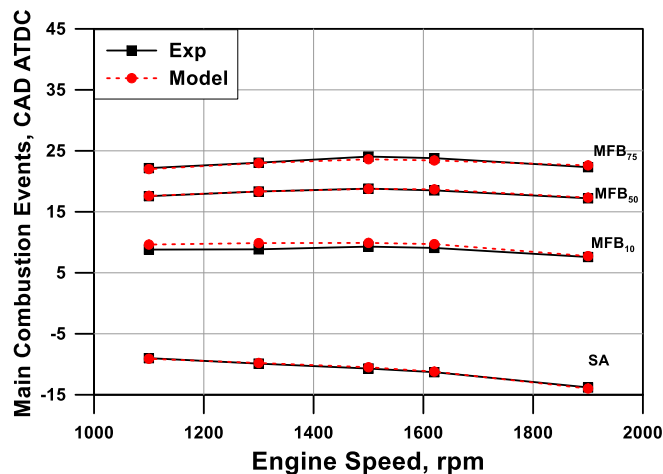
Figure 11. Experimental vs numerical comparison of characteristic combustion angles at full load.

6.3 Model validation

Once tuned at full load, the combustion model is applied to the analysis of all the other operating points listed in Table 2, using the same set of previously defined tuning constants. Firstly, the model validation is proved in terms of global performance, where the Root Mean Squared Error (RMSE) is presented as a global indicator of the model accuracy. To show the model sensitivity to the engine load, in Figure 12-Figure *18*, the five load levels tested at each speed (see Table 2) have been differenced by various symbols and colours.

In Figure 12 the measured and computed air flow rates are compared. The RMSE is rather low (10.92 kg/h) and all the analysed points are within the error band ± 5%, denoting an accurate schematization of the engine geometry, of the turbocharging system, and a proper specification of the valve flow coefficients.

The experimental/numerical correlation between the main combustion events is reported in Figure 13-Figure *14*, while in Figure 15 is showed the burn duration. Globally, the model produces with good accuracy the prediction of all these quantities. In particular, the SA is well-captured with an RMSE of about 1.15 CAD (Figure 13). Since the load spans from 20% to 100% of the full load, this result can be considered excellent, being the model capable to perceive the progressive advance of the spark timing at reducing load. This is obtained thanks to the ability to consider the superimposed effects of the simultaneous decrease of in-cylinder turbulence, pressure, and temperature. The good accuracy in the prediction of combustion phases for all load levels is further confirmed by Figure 14 in which the numerical/experimental correlation of MFB_{10} is shown. Even for the MFB_{10} the accuracy is very good, in fact, the error never exceeds ±2 CAD for all the prescribed loads, with an RMSE of 0.84 CAD.

The burn duration is again considered between 10% and 75% of the fuel burned. In Figure 15, the burn duration prediction is good in comparison with the measured counterparts, with an RMSE of 0.77 CAD, confirming the robustness of both combustion and turbulence models.
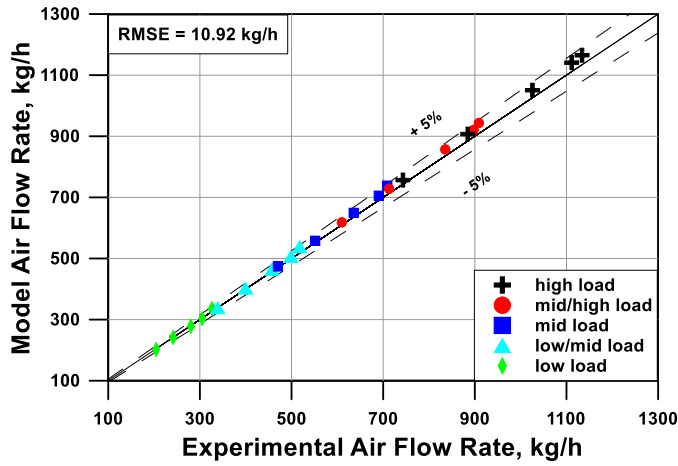
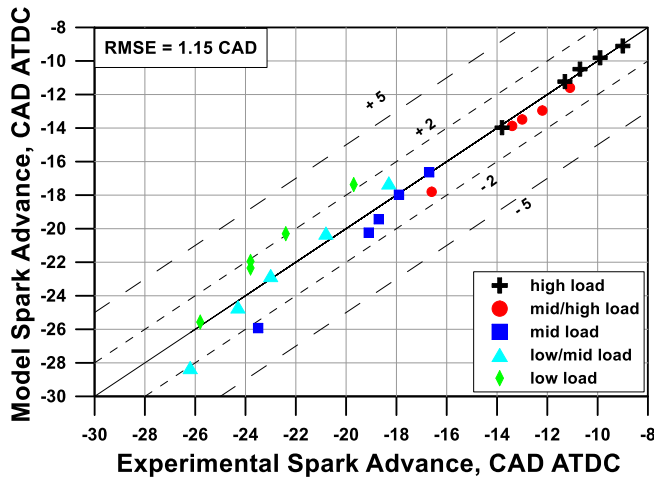**Figure 12**. Experimental vs numerical airflow rate comparison.

Figure 13. Experimental vs numerical spark advance comparison.

The above combustion results can be considered satisfactory, taking into account that no case-dependent tuning is applied, and the assessment includes both full and part load operating points. The globally appropriate accuracy in the combustion process description is confirmed by the numerical/experimental comparisons of peak pressure level, depicted in Figure 16. The peak pressure level is to some extent overestimated / underestimated at high / low-load, but always inside a range of ±5%, with an RMSE of 0.74 bar.
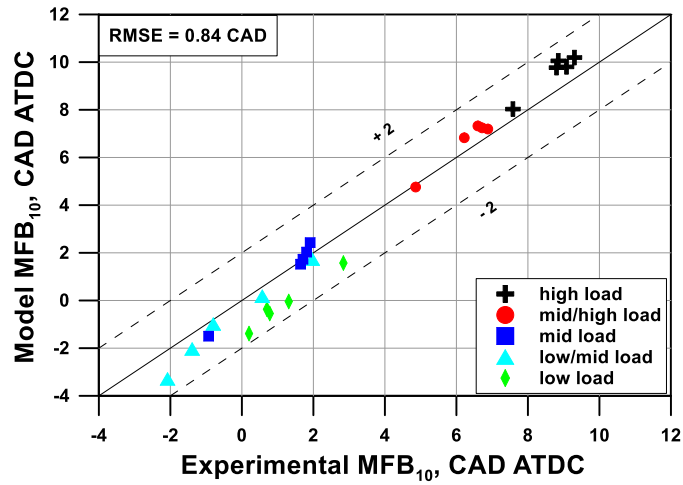
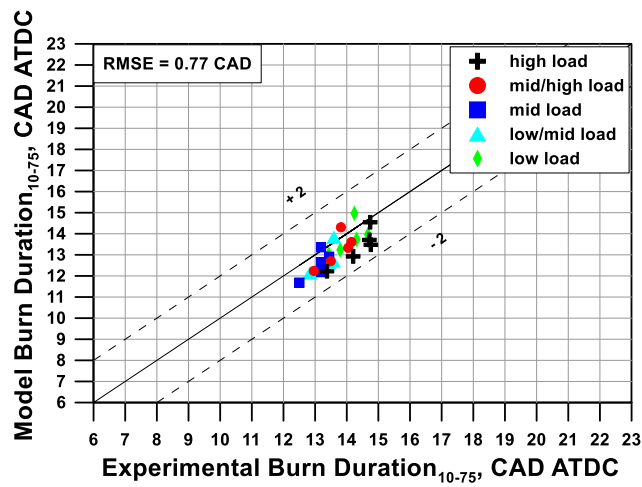**Figure 14**. Experimental vs numerical MFB 10 comparison.

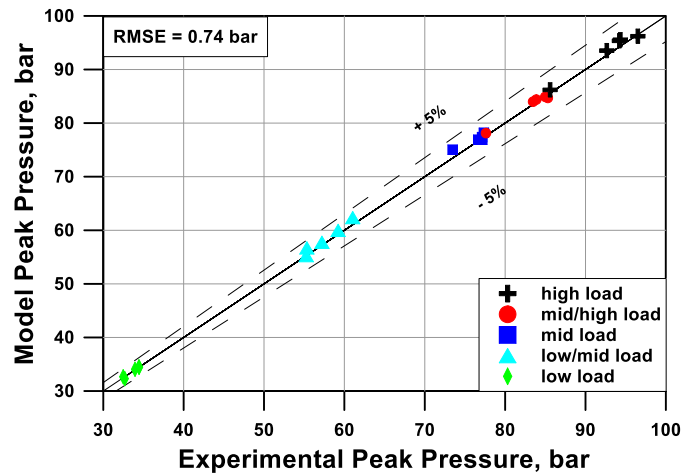**Figure 15**. Experimental vs numerical Burn Duration 10-75 comparison.

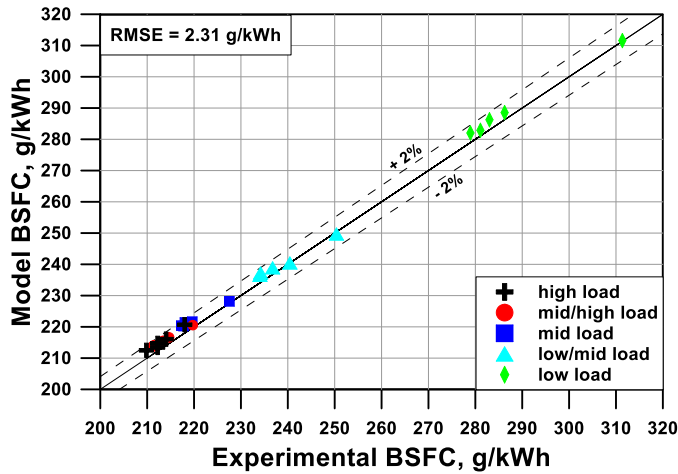**Figure 16**. Experimental vs numerical pressure peak comparison.

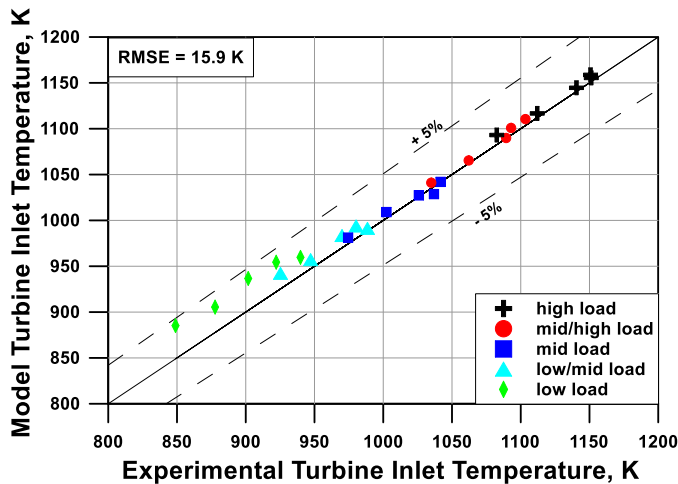**Figure 17**. Experimental vs numerical BSFC comparison.

Figure 18. Experimental vs numerical turbine inlet temperature.

As a further confirmation of the model reliability in terms of wall heat transfer, flow, and combustion prediction, the BSFC comparison is reported in Figure 17. All the operating points are included in the band ± 5%, with an RMSE equal to 2.31 g/kWh. The highest errors occur systematically at low loads, where the fuel consumption is slightly overestimated.

In Figure 18 the correlation between experimental data and numerical results on turbine inlet temperature is shown. The accuracy is good, with an RMSE equal to 15.9 K. A little overestimation for low load levels is observed, but numerical results are always in the range of ±5% of deviation, depicting a good calibration of both in-cylinder and exhaust pipes wall heat transfer.
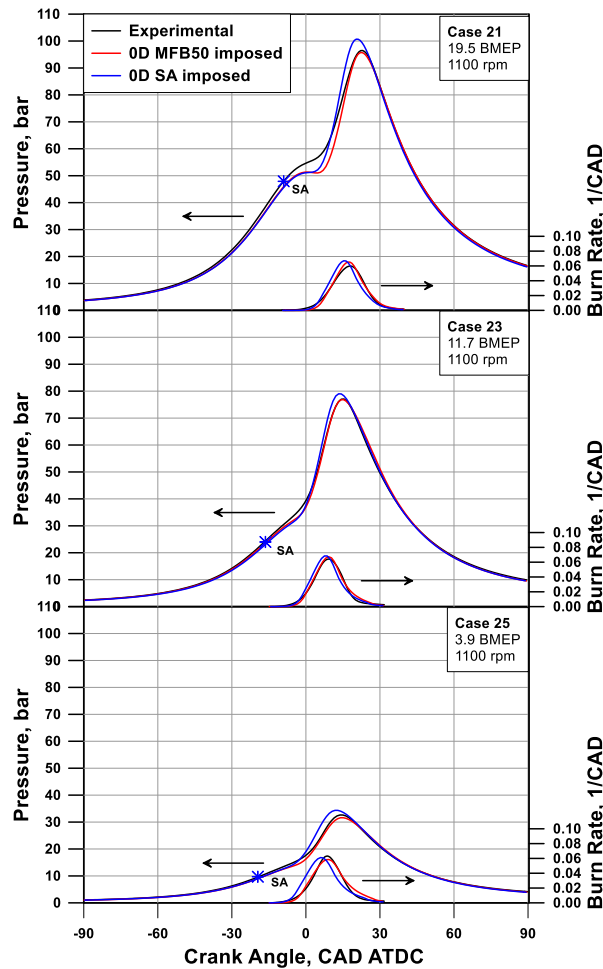
Figure 19. Experimental vs numerical comparison of in-cylinder pressure traces and burn rates at 1100rpm@ 19.5 (a), 11.7 (b), 3.9 (c) BMEP.

A more impressive check of the simulation reliability is given by the experimental/numerical comparisons of the pressure traces and the related burn rates, shown in Figure 19-Figure **21**. In particular, 9 representative operating points from Table 2 are selected, at different engine speeds and loads. The black lines represent the experimental traces, whereas the red ones correspond to the model outcomes. The comparison is done for mean pressure cycles, experimental traces are obtained for 200 firing cycles with a percentual error of 1%.

The agreement between experimental/numerical pressure trends is quite good in terms of global shape, timing and peak levels for all the analysed operating points. During the compression stroke, a slight underestimation of the pressure traces is visible with a higher extent at increasing load. The underestimation of the pressure traces could be probably due to the prediction of a slightly faster combustion, with delayed beginning, which reflects in lower pressure levels around the TDC. At this stage of the research, a model of kernel development is not considered, but this is expected to improve the model predictivity. Another possible reason for pressure mismatch around the TDC could be some inaccuracy in the experimental measurement of the boost level, which is targeted in the model by the turbocharger WG control. Regarding the burn rate, the model well follows the experimental profiles, detecting the evident slow-down when the load decreases. The demonstrated accuracy of the combustion model, as already

mentioned, mainly relies on the capability to perceive superimposed effects of in-cylinder, turbulence, pressure, temperature, and residual content.

For sake of completeness, 1D the simulations are repeated with experimental SA imposed and the corresponding results are plotted in Figure 19-Figure **21** with blue lines. In this case, the model tuning is kept unchanged to have a fair comparison with results with MFB$_{50}$ imposed. The figures put into evidence that the model accuracy slightly worsens when imposing the SA instead of the MFB$_{50}$. This modelling lack is expected to improve with a better description of the early combustion stage, including the flame kernel formation and development.
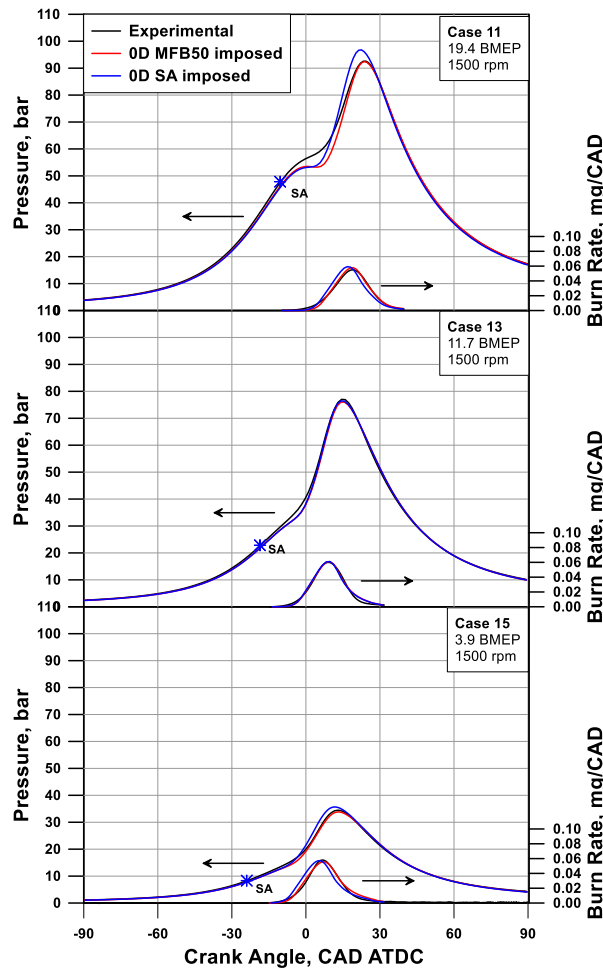

Figure 20. Experimental vs numerical comparison of in-cylinder pressure traces and burn rates at 1500 rpm@ 19.4 (a), 11.7 (b), 3.9 (c) BMEP.
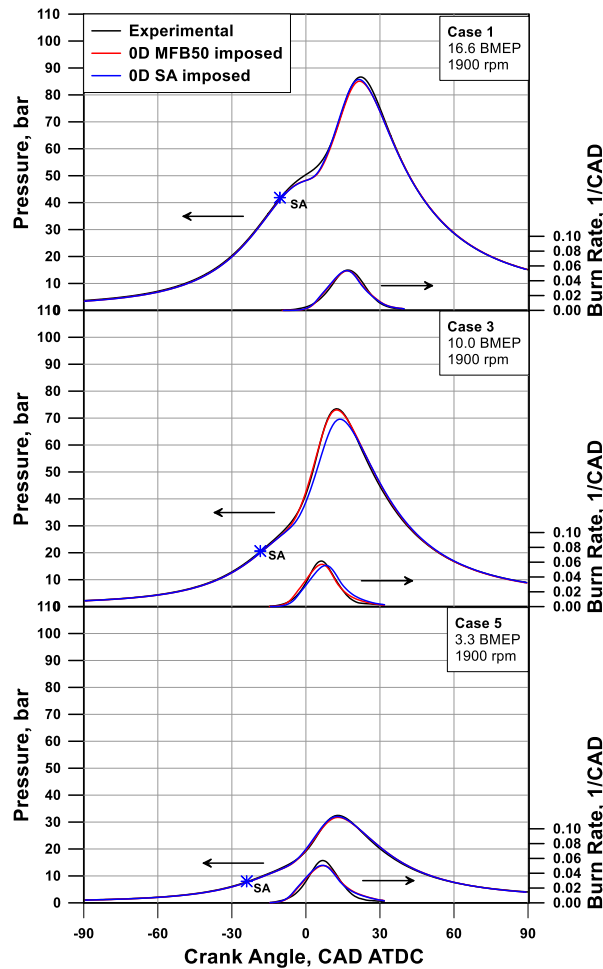
Figure 21. Experimental vs numerical comparison of in-cylinder pressure traces and burn rates at 1900 rpm@ 16.6 (a), 10.0 (b), 3.3 (c) BMEP.

7. Conclusions

The main topic of this work was to use the predictive capabilities of a fractal combustion model, through the coupling with an appropriate turbulence model suitable for large bore engines, including swirl motion interacting with the squish motion as a turbulence production source in addition to tumble collapse. The developed models are adopted to simulate the operation of an SI CNG heavy-duty engine retrofitted from a CI Diesel engine, where the intake port and piston shape are conceived to promote swirl motion within the cylinder.

The turbulence model is hence embedded in a phenomenological combustion model to simulate the engine behaviour under various operating conditions, different in terms of rotational speed and load. Once tuned, the fractal model accuracy was verified in terms of both global performance, combustion phasing, and pressure traces against an extensive experimental dataset composed of 25 operating points. The results underlined the model capability in predicting air flow rate and BSFC, with a reasonable error band of ±2%. Concerning the pressure traces and the burn rates, the experimental/numerical agreement is satisfactory in all operating points. This also reflects in a good prediction of the main combustion events and durations. It is worth underlining that the results were obtained using a unique set of tuning constants for all

the operating points, demonstrating that the physics behind the model is accurate enough to utilize it in a predictive way.

Acronyms

0D/1D/3D	Zero/One/Three–Dimensional
AFTDC	After Firing Top dead center
BFTDC	Before Firing Top dead center
BMEP	Brake mean effective pressure
BSFC	Brake specific fuel consumption
CAD	Crank angle degree
CFD	Computational Fluid Dynamics
CI	Compression Ignition
CNG	Compressed Natural Gas
EGR	Exhaust Gas Recirculation
EOI	End of Injection
FMEP	Friction Mean Effective Pressure
FTDC	Firing Top dead center
HD	Heavy Duty
ICE	Internal Combustion Engine
IMEP	Indicated Mean Effective Pressure
LNG	Liquefied Natural Gas
MFB	Mass fraction burned
MPI	Multi Point Injection
PTG	Power-to-Gas
RMSE	Root Mean Square Error
SA	Spark advance
SI	Spark ignition
TCO	Total Cost Ownership
TDC	Top Dead Center
TKE	Turbulent Kinetic Energy

Symbols

A_L	Flame front laminar area
A_T	Flame front turbulent area
B	Cylinder bore
B_q	Characteristic dimension of in-cylinder charge along radial direction

$c_{fd0,S}$, $c_{fdm,S}$	Tuning constants of swirl decay function
$c_{fd0,T}$, $c_{fdm,T}$	Tuning constants of tumble decay function
c_{Kin0}	Tuning constant of inlet flow coefficient
c_{PKk}	Tuning constant of turbulent production
$c_{r0,S}$, $c_{rm,S}$	Parameters for swirl radius adjustment
$c_{r0,T}$, $c_{rm,T}$	Parameters for tumble radius adjustment
c_{Sin}, c_{Sex}	Tuning constants of swirl flow coefficient
c_{Tin0}	Tuning constant of tumble flow coefficient
D_3	Flame front fractal dimension
d_{bowl}	Piston bowl diameter
$f_{d,S}$	Decay function of swirl
$f_{d,T}$	Decay function of tumble
H	Piston position referred to cylinder head
k	Turbulent kinetic energy
K	Mean flow kinetic energy

K_S	Kinetic energy related to swirl motion
k_{sq}	Kinetic energy related to squish motion
K_S	Kinetic energy related to swirl motion
K_T	Kinetic energy related to tumble motion
L_i	Integral Length Scale
L_{max}	Flame wrinkling maximum scale
L_{min}	Flame wrinkling minimum scale
m	Mass
N_{swirl}	Swirl number
N_{tumble}	Tumble number
P	Turbulence production
p	Pressure
r_S	Swirl radius
r_T	Tumble radius
S	Swirl momentum
s_{bowl}	Piston bowl height
S_L	Laminar flame speed
S_{L0}	Unstretched Laminar flame speed
S_T	Turbulent flame speed

t	Time
T	Temperature, Tumble momentum
t_S	Characteristic time scale of swirl
t_T	Characteristic time scale of tumble
t_{TS}	Weighted average characteristic time scale
U	Mean flow velocity
u'	Turbulence intensity
U_a	Axial mean flow velocity
U_r	Radial mean flow velocity
U_S	Swirl velocity
U_{sq}	Squish velocity
U_T	Tumble velocity
v	Flow velocity throughout the valve
$V(\theta)$	Instantaneous combustion chamber volume
V_{cyl}	Cylinder volume

Greeks

α Temperature ratio exponent of laminar flame speed correlation

β Pressure ratio exponent of laminar flame speed correlation

φ Air/fuel equivalence ratio

ε Dissipation rate

λ Relative air-to-fuel ratio

v_t Turbulent viscosity

ρ Density

ω Angular velocity

Subscripts

0   Room conditions

10 / 50 / 90   Referring to 10 / 50 / 90% of mass fraction burned

b   Burned

eng   Referred engine

exb   Backward flow through the exhaust valve

exf   Forward flow through the exhaust valve

inb   Backward flow through the intake valve

inc   Incoming flow inside the cylinder

inf   Forward flow through the intake valve

K	Related to mean flow kinetic energy
max	Maximum value
min	Minimum value
out	Outcoming flow from the cylinder
S	Related to swirl motion
T	Related to tumble motion
u	Unburned

Superscripts

.	Time derivative

References

1. Steffen, W., Broadgate, W., Deutsch, L., Gaffney, O., et al. "The trajectory of the Anthropocene: The Great Acceleration", The Anthropocene Review, 1-18, 2015, doi: 10.1177/2053019614564785.
2. Annual European Union greenhouse gas inventory 1990–2020 and inventory report 2022, https://www.eea.europa.eu//publications/annual-european-union-greenhouse-gas-1
3. 'IARC: diesel engine exhaust carcinogenic', International Agency for Research on Cancer, Press Release No. 213, 12th June, 2012.
4. Alamia, A., Magnusson, I., Johnsson, F., & Thunman, H., "Well-to-wheel analysis of bio-methane via gasification, in heavy duty engines within the transport sector of the European Union." Applied energy, 2016, 170, 445-454, doi:10.1016/j.apenergy.2016.02.001
5. Blanco, H., Nijs, W., Ruf, J., Faaij, A., "Potential of Power-to-Methane in the EU energy transition to a low carbon system using cost optimization," Applied energy, 2018, 232, 323-340, doi:10.1016/j.apenergy.2018.08.027.
6. Wheeler, J., Stein, J., and Hunter, G., "Effects of Charge Motion, Compression Ratio, and Dilution on a Medium Duty Natural Gas Single Cylinder Research Engine," SAE Int. J. Engines 7(4):1650-1664, 2014, doi:10.4271/2014-01-2363.
7. Johansson, B. and Olsson, K., "Combustion Chambers for Natural Gas SI Engines Part I: Fluid Flow and Combustion," SAE Tech. Pap. 950469, 1995, doi:10.4271/950469.
8. Heywood, J., B., "Internal combustion engine fundamentals," Vol. 930, New York, Mcgraw-Hill, 1988, ISBN: 007028637X.
9. Borgnakke, C., Arpaci, V., and Tabaczynski, R., "A Model for the Instantaneous Heat Transfer and Turbulence in a Spark Ignition Engine," SAE Technical Paper 800287, 1980, doi:10.4271/800287.
10. Morel, T. and Mansour, N., "Modeling of Turbulence in Internal Combustion Engines," SAE Technical Paper 820040, 1982, doi:10.4271/820040.
11. Morel, T. and Keribar, R., "A Model for Predicting Spatially and Time Resolved Convective Heat Transfer in Bowl-in-Piston Combustion Chambers," SAE Technical Paper 850204, 1985, doi:10.4271/850204.
12. Grasreiner, S., Neumann, J., Luttermann, C., Wensing, M. et al., "A Quasi-Dimensional Model of Turbulence and Global Charge Motion for Spark Ignition Engines with Fully Variable Valvetrains," International Journal of Engine Research 15(7):805-816, 2014, doi:10.1177/1468087414521615.
13. Fogla, N., Bybee, M., Mirzaeian, M., Millo, F. et al., "Development of a K-k-ε Phenomenological Model to Predict In-Cylinder Turbulence," SAE Int. J. Engines 10(2):562-575, 2017, doi:10.4271/2017-01-0542.
14. Bozza, F., De Bellis, V., Berni, F., D'Adamo, A. et al., "Refinement of a 0D Turbulence Model to Predict Tumble and Turbulent Intensity in SI Engines. Part I: 3D Analyses," SAE Technical Paper 2018-01-0850, 2018, doi:10.4271/2018-01-0850.
15. De Bellis, V., Bozza, F., Fontanesi, S., Severi, E. et al., "Development of a Phenomenological Turbulence Model through a Hierarchical 1D/3D Approach Applied to a VVA Turbocharged Engine," SAE Int. J. Engines 9(1):506-519, 2016, doi:10.4271/2016-01-0545.
16. Bozza, F., Teodosio, L., De Bellis, V., Fontanesi, S. et al., "Refinement of a 0D Turbulence Model to Predict Tumble and Turbulent Intensity in SI Engines. Part

II: Model Concept, Validation and Discussion," SAE Technical Paper 2018-01-0856, 2018, doi:10.4271/2018-01-0856.

17. Kim, M., Kim, Y., Kim, J., Song, H. H., "Development of quasi-dimensional turbulence model for spark-ignition engine with physical analysis of tumble: Energy-based tumble model focusing on energy intake and turbulence production," Applied Energy, 2019, 252, 113455, doi.org/10.1016/j.apenergy.2019.113455

18. Bozza, F., Teodosio, L., De Bellis, V., Fontanesi, S. et al., "A Refined 0D Turbulence Model to Predict Tumble and Turbulence in SI Engines," SAE Int. J. Engines 12(1):2019, doi:10.4271/03-12-01-0002.

19. De Bellis, V., Severi, E., Fontanesi, S., Bozza, F., "Hierarchical 1D/3D approach for the development of a turbulent combustion model applied to a VVA turbocharged engine. Part II: Combustion model", Energy Procedia 45: 1027-1036, 2014.

20. De Bellis, V., Bozza, F., Tufano, D., "A Comparison Between Two Phenomenological Combustion Models Applied to Different SI Engines," SAE Technical Paper, 2017-01-2184, doi:10.4271/2017-01-2184.

21. Matthews, R. and Chin, Y., "A Fractal-Based SI Engine Model: Comparisons of Predictions with Experimental Data," SAE Technical Paper 910079, 1991, doi:10.4271/910079.

22. Poulos, S. and Heywood, J., "The Effect of Chamber Geometry on Spark-Ignition Engine Combustion," SAE Technical Paper 830334, 1983, doi:10.4271/830334.

23. Demesoukas, S., Caillol, C., Higelin, P., and Boiarciuc, A., "Zero-Dimensional Spark Ignition Combustion Modeling - A Comparison of Different Approaches," SAE Technical Paper 2013-24-0022, 2013, doi:10.4271/2013-24-0022.

24. Richard, S., Bougrine, S., Font, G., Lafossas, F.A., Le Berr, F., "On the Reduction of a 3D CFD Combustion Model to Build a Physical 0D Model for Simulating Heat Release, Knock and Pollutants in SI Engines", Oil & Gas Science and Technology 64(3):223-242, 2009, doi:10.2516/ogst/2008055.

25. Perlman, C., Frojd, K., Seidel, L., Tuner, M. et al., "A Fast Tool for Predictive IC Engine In-Cylinder Modelling with Detailed Chemistry," SAE Technical Paper 2012-01-1074, 2012, doi:10.4271/2012-01-1074.

26. Rakopoulos, C., Michos, C., and Giakoumis, E., "Thermodynamic Analysis of SI Engine Operation on Variable Composition Biogas-Hydrogen Blends Using a Quasi-Dimensional, Multi-Zone Combustion Model," SAE Int. J. Engines 2(1):880-910, 2009, doi:10.4271/2009-01-0931.

27. Verhelst, S., Sheppard, C., G., W., "Multi-zone thermodynamic modelling of spark-ignition engine combustion-an overview", Energy Conversion and management 50(5): 1326-1335, 2009, doi: https://doi.org/10.1016/j.enconman.2009.01.002.

28. Franke, C., Wirth, A., Peters, N., "New Aspects of the Fractal Behaviour of Turbulent Flames", 23 Symp. (Int.) on Combustion, Orleans, 1990.

29. Gatowsky, J., A., Heywood, J., B., "Flame Photographs in a Spark-Ignition Engine", Combustion and Flame 56:71-81, 1984.

30. Gouldin, F., "An application of Fractals to Modeling Premixed Turbulent Flames", Combustion and Flame 68(3):249-266, 1987, doi:10.1016/0010-2180(87)90003-4.

31. Bozza, F., Teodosio, L., De Bellis, V., Fontanesi, S. et al., "A Refined 0D Turbulence Model to Predict Tumble and Turbulence in SI Engines," SAE Int. J. Engines 12(1):2019, doi:10.4271/03-12-01-0002.

32. Bozza, F., De Bellis, V., Berni, F., D'Adamo, A. et al., "Refinement of a 0D Turbulence Model to Predict Tumble and Turbulent Intensity in SI Engines. Part I: 3D Analyses," SAE Technical Paper 2018-01-0850, 2018, doi:10.4271/2018-01-0850.

33. Franken, T., Sommerhoff, A., Willems, W., Matrisciano, A. et al., "Advanced Predictive Diesel Combustion Simulation Using Turbulence Model and Stochastic Reactor Model," SAE Technical Paper 2017-01-0516, 2017, doi:10.4271/2017-01-0516.

34. Riccardi, M., De Bellis, V., Sforza, L., Beatrice, C. et al., "Advanced Turbulence Model for SI Combustion in a Heavy-Duty NG Engine," SAE Technical Paper 2022-01-0384, 2022, https://doi.org/10.4271/2022-01-0384.

35. Lucchini, T., D'Errico, G., Paredi, D., Sforza, L. et al., "CFD Modeling of Gas Exchange, Fuel-Air Mixing and Combustion in Gasoline Direct-Injection Engines," SAE Technical Paper 2019-24-0095, 2019, doi:10.4271/2019-24-0095

36. Sforza, L., Lucchini, T., Gianetti, G., and D'Errico, G., "Development and Validation of SI Combustion Models for Natural-Gas Heavy-Duty Engines," SAE Technical Paper 2019-24-0096, 2019, doi:10.4271/2019-24-0096

37. Sforza, L., Lucchini, T., Gianetti, G., D'Errico, G. et al., "A 3D-CFD Methodology for Combustion Modeling in Active Prechamber SI Engines Operating with Natural Gas," SAE Technical Paper 2022-01-0470, 2022, doi:10.4271/2022-01-0470

38. Franke, C., Wirth, A., Peters, N., "New Aspects of the Fractal Behaviour of Turbulent Flames", 23 Symp. (Int.) on Combustion, Orleans, 1990.

39. Gatowsky, J., A., Heywood, J., B., "Flame Photographs in a Spark-Ignition Engine", Combustion and Flame 56:71-81, 1984.

40. North, G., L., Santavicca, D., A., "The fractal nature of premixed turbulent flames," Combustion Science and Technology 72(4-6): 215-232, 1990, doi:10.1080/00102209008951648.

41. De Bellis, V., Bozza, F., Tufano, D., "A Comparison Between Two Phenomenological Combustion Models Applied to Different SI Engines," SAE Technical Paper, 2017-01-2184, doi:10.4271/2017-01-2184.

42. Amirante, R., Distaso, E., Tamburrano, P., Reitz, R. D, "Laminar flame speed correlations for methane, ethane, propane and their mixtures, and natural gas and gasoline for spark-ignition engine simulations," International Journal of Engine Research, 18(9), 951-970, 2017, doi: 10.1177/1468087477720018.

43. Amirante, R., E. Distaso, P. Tamburrano, R. D. Reitz. "Analytical correlations for modeling the laminar flame speed of natural gas surrogate mixtures," Energy Procedia 126 (2017): 850-857, doi: 10.1016/j.egypro.2017.08.289.

44. Riccardi, M., Tufano, D., Beatrice, C., Bozza, F. et al., "Toward Predictive Combustion Modeling of CNG SI Engines in 1D Simulation Tools," SAE Technical Paper 2020-01-2079, 2020, https://doi.org/10.4271/2020-01-2079.

45. Teodosio, L., De Bellis, V., Bozza, F., "Combined Effects of Valve Strategies, Compression Ratio, Water Injection, and Cooled EGR on the Fuel Consumption of a Small Turbocharged VVA Spark-Ignition Engine," SAE International Journal of Engines, 11(6), 643-656, doi:https://www.jstor.org/stable/26649121.

46. De Bellis, V., Bozza, F., Tufano, D., "A Comparison Between Two Phenomenological Combustion Models Applied to Different SI Engines," SAE Technical Paper, 2017-01-2184, doi:10.4271/2017-01-2184.

47. De Bellis, V., Malfi, E., Teodosio, L., Giannattasio, P., & Di Lenarda, F., "A Novel Laminar Flame Speed Correlation for the Refinement of the Flame Front

Description in a Phenomenological Combustion Model for Spark-Ignition Engines," SAE International Journal of Engines, 12(3), 251-271, 2019.

48. Blizard, N., Keck, J., "Experimental and Theoretical Investigation of Turbulent Burning Model for Internal Combustion Engines", SAE paper 740191, 1974, doi: 10.4271/740191.

49. Keck, J., Heywood, J., Noske, G., "Early Flame Development and Burning Rates in Spark Ignition Engines and Their Cyclic Variability", SAE Technical Paper 870164, 1987, doi:10.4271/870164.

50. Peters, N., "Laminar flamelet concepts in turbulent combustion", Symposium (International) on Combustion 21(1): 1231-1250, 1988, doi: 10.1016/S0082-0784(88)80355-2.

51. Bates, C. S., "Flame Imaging Studies of Combustion Completion in a SI Four-Stroke Engine", TvU Thoughtventions Unlimited LLC, http://www.tvu.com/.